

OBSERVATIONS OF Mg II ABSORPTION NEAR $z \sim 1$ GALAXIES SELECTED FROM THE DEEP2 REDSHIFT SURVEY¹

ELIZABETH LOVEGROVE^{2,3}, ROBERT A. SIMCOE^{2,4}

Draft version February 24, 2024

ABSTRACT

We study the frequency of Mg II absorption in the outer haloes of galaxies at $z = 0.6 - 1.4$ (with median $z = 0.87$), using new spectra obtained of ten background quasars with galaxy impact parameters of $b < 100$ kpc. The quasar sightlines were selected from the SDSS DR6 QSO catalog based on proximity to galaxies in the DEEP2 redshift survey. In addition to the 10 small impact systems, we examine 40 additional galaxies at $100 < b < 500$ kpc serendipitously located in the same fields. We detect Mg II absorbers with equivalent width $W_r = 0.15 \text{ \AA} - 1.0 \text{ \AA}$, though not all absorbers correlate with DEEP galaxies. We find five unique absorbers within $\Delta v = 500$ km/s and $b < 100$ kpc of a DEEP galaxy; this small sample contains both early and late type galaxies and has no obvious trends with star formation rate. No Mg II is detected more than 100 kpc from galaxies; inside this radius the covering fraction scales with impact parameter and galaxy luminosity in very similar fashion to samples studied at lower redshift. In all but one case, when Mg II is detected without a spectroscopically confirmed galaxy, there exists a plausible photometric candidate which was excluded because of slit collision or apparent magnitude. We do not detect any strong absorbers with $W_r > 1.0 \text{ \AA}$, consistent with other samples of galaxy-selected Mg II systems. We speculate that Mg II systems with $0.3 < W_r < 1.0$ trace old relic material from galactic outflows and/or the halo assembly process, and that in contrast, systems with large W_r are more likely to reflect the more recent star forming history of their associated galaxies.

1. INTRODUCTION

For roughly two decades, a connection has been observed between $\sim L^*$ galaxies and the Mg II absorption systems seen in QSO spectra (Bergeron & Boissé 1991; Steidel et al. 1994; Steidel & Sargent 1992). Mg II systems trace gas in the outer haloes of these objects out to radii of ~ 100 kpc. However, a standardized physical picture describing the origin of this metal-rich material remains elusive. At least two different pathways have been suggested for distributing Mg II throughout galaxy haloes.

In one scenario, the QSO absorbers represent debris from large-scale winds that are seen in galaxy spectra and known to carry Mg II (Weiner et al. 2009; Bond et al. 2001). These winds may help quench star formation in nascent galaxies, providing necessary feedback in galaxy formation models. For example, Nestor et al. (2010) associated ultrastrong absorbers ($W_r \geq 3 \text{ \AA}$) with starbursting galaxies and suggested an outflow wind scenario based on velocity dispersions in the Mg II systems. Prochter et al. (2006) favored an outflow model of Mg II systems based on evolutionary trends with redshift in the number density of (strong) absorbers. Some theories associate these outflows with AGN activity rather than supernova feedback, but differentiation between the two remains an open question.

Several authors have argued indirectly in favor of this interpretation as well. Bouché et al. (2006) detected evidence that stronger Mg II absorbers reside in lower

mass galaxy haloes, and suggested that this might result from the more vigorous star formation occurring in the smaller, late-type galaxies. Using various statistical combinations of SDSS Mg II absorbers, Zibetti et al. (2007) and Ménard et al. (2009) reported evidence of star formation surrounding the strongest Mg II systems, in the form of enhanced [OII] emission or bluer galaxy colors.

However, a second interpretation posits that Mg II systems are a generic feature of galaxy haloes, with an extent and dynamical structure that reflects gravitational processes. Indeed the velocity profiles of some Mg II systems appear to form an extension of galactic rotation curves (Kacprzak et al. 2010; Steidel et al. 2002), albeit with increased velocity dispersion. Chen & Tinker (2008) and Chen et al. (2010) develop a halo-motivated model using a large set of QSO-galaxy pairs. These papers and Gauthier et al. (2009) interpret the anti-correlation between galaxy halo mass and Mg II strength in the context of the “cold mode” vs. “hot mode” accretion models recently advocated by Kereš et al. (2005); Dekel et al. (2009). In this model, Mg II absorption arises in cold structures that are ionized away when galaxy masses - and hence virial temperatures - exceed a threshold value. In a carefully selected sample, Chen & Tinker (2008) find absorbers associated with both early- and late-type galaxies in normal field proportions, and use this to argue against an interpretation where Mg II arises exclusively in starburst galaxies.

Galaxy-absorber studies to date have primarily focused on low redshifts $z \lesssim 0.5$ where galaxy observations are most accessible (Chen et al. 2010), or on targeted galaxy observations toward sightlines pre-selected for Mg II absorption (Kacprzak et al. 2010; Nestor et al. 2005; Steidel et al. 2002). A uniform interpretation of

¹ This paper includes data gathered with the 6.5 meter Magellan Telescopes located at Las Campanas Observatory, Chile.

² MIT-Kavli Center for Astrophysics and Space Research

³ University of California, Santa Cruz

⁴ Sloan Foundation Research Fellow

the results is also complicated by the different samples' varying sensitivities, completeness estimates, and selection techniques.

In this paper, we construct a modest sample for studying Mg II -galaxy associations at higher redshift ($0.6 < z < 1.4$). To do this, we leverage the public catalog of the DEEP2 redshift survey (Davis et al. 2003, 2007) and use the MagE spectrometer on Magellan to obtain spectra of background QSOs that lie randomly near DEEP2 galaxies on the sky.

Since this galaxy sample is chosen without regard to morphology, it is not biased toward any spectral type or the presence/absence of AGN; thus, it should be appropriate for investigating the relationship between Mg II incidence, star formation, and spectral/morphological type. The sample also spans a wide range of impact parameters, allowing for an estimate of how the Mg II covering fraction scales with galactic radius. The DEEP sample does pre-select galaxies based on color and magnitude and is known to preferentially select star forming galaxies at high redshift (Gerke et al. 2007a). However, it provides a large, uniformly selected parent sample against which we can compare a subsample drawn randomly based only on impact parameter.

In Section 2, we describe our sample selection and observations. Section 3 details the galaxy-Mg II pairs detected as well as non-detections. Section 4 describes our results in the context of the existing literature. We use a Λ CDM cosmology of $\Omega_m = 0.272$, $\Omega_\Lambda = 0.728$, $H_0 = 70.4 \text{ km s}^{-1} \text{ Mpc}^{-1}$ throughout. All magnitudes are on the AB system, and impact parameters are listed in proper $h_{71}^{-1} \text{ kpc}$.

2. OBSERVATIONS

Our objective is to assemble a sample of galaxy-absorber pairs at moderate redshift where the galaxy sample is *not* selected based on pre-existing knowledge of the presence of Mg II absorption. This method has been employed successfully at lower redshifts but becomes somewhat less practical at higher z because of the expense and incompleteness of the galaxy observations. To work around this limitation, we started with the well-defined, public galaxy redshift catalog of the DEEP2 survey, which contains galaxies at $0.6 < z < 1.4$. We then selected for observation all quasars in the SDSS DR6 catalog whose sightlines passed less than 100 kpc from a DEEP2 galaxy. All quasars meeting this criterion were observed.

This method generates a randomized galaxy-absorber pair sample, since inclusion depends only on the relative position of the two objects. The galaxies and QSOs will retain the selection functions of their respective surveys, which are unrelated to our present science goals. The quasars are being used for background illumination only. Although the galaxy parent catalog reflects DEEP2's selection process, we show in Section 2.3 that it contains a mixture of spectral classes (i.e. both star forming and early type) and hence may be used to study the association of star formation with Mg II incidence.

We choose Mg II because it has been studied extensively at lower redshift, and it falls directly in the optical window through DEEP2's redshift window. Ly α falls below the 3000 Å atmospheric cutoff. C IV could be visible at the high redshift end of the sample, but this range

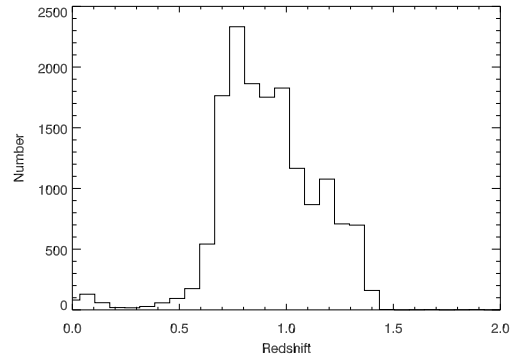


FIG. 1.— The redshift distribution of DEEP2 galaxies in the equatorial fields.

contains few galaxy-sightline pairs and our observations did not yield any galaxy-absorber pairs where C IV would be visible. In one case we detect Fe II in conjunction with Mg II.

2.1. Quasar Selection

To select target quasars for observation, we cross correlated the DEEP2 DR3 public redshift catalog⁵ (containing $\sim 46,000$ objects) with the DR6 quasar catalog produced by the SDSS. Magellan access necessitated restricting our targetable declination range to the two equatorial fields in DEEP2. We also required that $z_{QSO} > 1.0$, i.e. that the quasar lie behind much of the DEEP2 survey. These cuts yielded a final tally of 46 Sloan quasars.

For each of these quasars, we then identified all galaxies from the DEEP2 catalog having impact parameters of 30'' or less from the quasar's line of sight. We excluded all galaxies with a "redshift quality" flag of 2 or lower as unreliable, following the recommendation of the DEEP2 DR3 website. Only galaxies with $0.6 < z_{\text{galaxy}} < z_{QSO}$ were considered for each quasar.

Figure 1 shows the DEEP2 redshift histogram; in this range the angular diameter scale subtended per arcsecond ranges from 6.7 to $8.5 h_{70}^{-1} \text{ kpc}$. For a fiducial angular scale of 8 kpc per arcsecond, a 100 kpc impact parameter therefore corresponds to 12.5 arcseconds on the sky. Ten SDSS sightlines intercept a galaxy within this radius; these quasars form the core sample observed at Magellan.

Although not selected to do so, these same sightlines also serendipitously pass by other galaxies at larger impact parameter. The sample is much less complete at these larger radii, but it does contain 5 galaxies with $100 < b < 200 \text{ kpc}$, and many more at larger radii.

2.2. Quasar Observation

The ten SDSS quasars were each observed with the MagE spectrograph on the Magellan Clay telescope. The median QSO in our sample has $g' = 20$, with the total sample ranging from $17.95 < g' < 21.2$. MagE is a moderate resolution UV/optical echellette that delivers spectra from 3100 Å to $1 \mu\text{m}$ (Marshall et al. 2008). A 0.7 arcsecond slit was used, corresponding to a resolution of $R = 6000$, or 50 km/s. The observations were taken under photometric conditions during January and October

⁵ <http://deep.berkeley.edu>

TABLE 1
MAGE QUASAR OBSERVATIONS

SDSS Object	z_{QSO}	g'	Exp. Time (s)
233023+0008	1.00	19.92	2×1200
023101+0024	1.05	20.92	5×1200
232536+0019	1.21	19.78	4×1200
232634+0021	1.25	20.71	3×1200
023123+0044	1.26	20.30	6×1200
232632-0003	1.27	20.32	2×1200
023144+0052	1.61	20.58	4×1200
022639+0043	1.66	20.41	2×1200
232707+0003	1.75	20.55	2×1200
233050+0015	1.94	20.01	2×1200

of 2008. Table 1 lists observed quasars along with total exposure times.

Raw data from the spectrograph were processed using the MASE IDL pipeline (Bochanski et al. 2009). MASE performs poisson-limited sky subtraction on the 2D echelle frames using a wavelength-sampled grid. Object profiles are optimally extracted while iteratively converging to a joint model of the object and sky for each exposure. The unbinned extracted spectra are then combined and finally projected onto a regular wavelength grid. The final spectra exhibit signal-to-noise ratios ranging from 5 to 23 with a mean of 11.6 per pixel over the $\lambda = 4500 - 6700 \text{ \AA}$ range relevant to the detection of Mg II in our redshift search range.

2.3. Galaxy Sample

Our sample of galaxies is drawn solely from the DEEP2 survey, DR3. From this catalog, we selected the 5 nearest galaxies for each sightline, 50 in total. The impact parameter of the most distant galaxy therefore varies between fields but is no less than $250h_{71}^{-1} \text{ kpc}$ for any field. The resulting galaxy sample spans $0.662 \leq z \leq 1.409$ with a median of 0.868. Its color distribution is roughly uniform, containing galaxies at extremes of both the red and blue ends of DEEP’s selection region. Figure 2 shows the overall DEEP survey color distribution, with galaxies chosen for this sample highlighted. The color distribution of Mg II candidate galaxies is consistent with a random draw from DEEP2, in the group passing the color cuts. To confirm this, we ran a 2-sample, 2-dimensional Kolmogorov-Smirnov (KS) test on the distributions of $(R - I)$ and $(B - R)$ colors. The KS test admits the possibility (i.e. rules out at only the $P = 25\%$ level) that our sample and the full DEEP2 $0.6 < z < 1.4$ sample are drawn from the same color space. Likewise a one-dimensional two sample KS test on the redshift distribution fails to distinguish between our sample and that of DEEP2 in our redshift range ($P = 30\%$).

We have excluded DEEP2 objects in the Extended Groth Strip (EGS), where different selection criteria were used; we do not observe any QSOs in the EGS because of its northern declination and so have no Mg II candidates within this group.

The 50 galaxy spectra extracted from the DEEP archive were inspected in order to search for AGN signatures, and two candidates were identified: one definite (31049930), which displays strong Ne III and Ne V lines and a broad O II peak; and one very likely (31020054), which displays strong Ne III lines and a broad O II peak.

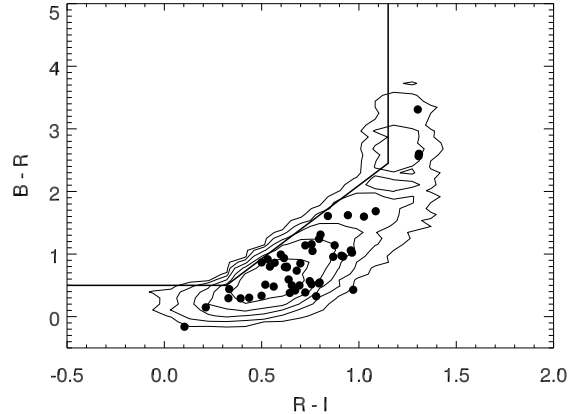


FIG. 2.— Color space distribution of spectroscopically confirmed DEEP2 DR3 galaxies, shown in density contours for clarity. Galaxies included in our sample are shown as solid dots. The DEEP photometric cuts define the upper left diagonal boundary of the distribution. Our Mg II sample galaxies span the full range of galaxies passing the color cuts, and are statistically consistent with a random draw from the survey.

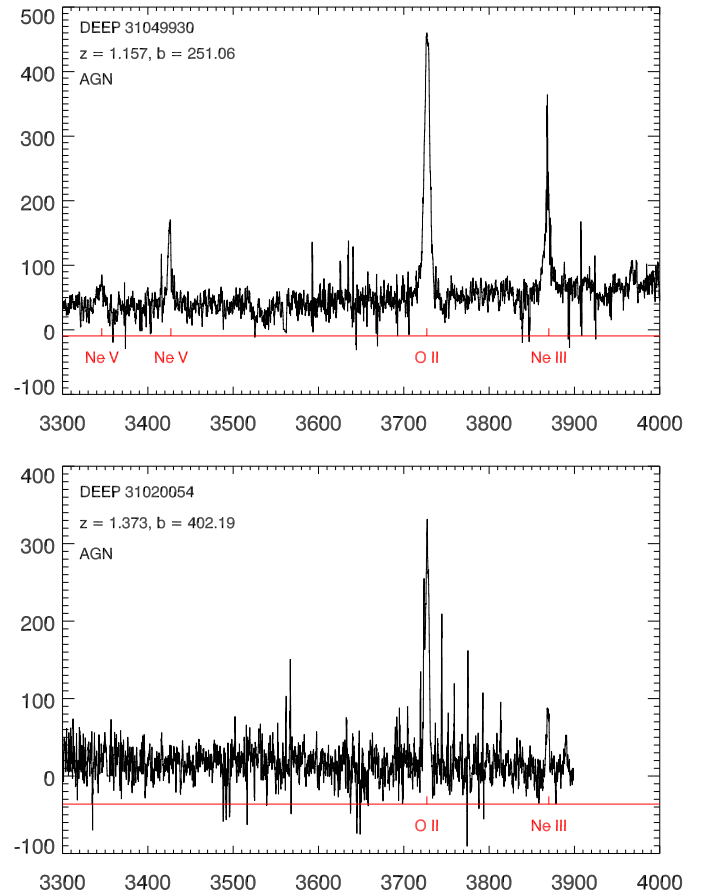


FIG. 3.— Spectra of AGNs in sample. 31049930 displays a broadened O II peak, strong Ne III, and strong Ne V. 31020054 displays a broadened O II doublet and Ne III peak.

These spectra can be seen in Figure 3. This gives an AGN fraction of 4% of the population. Neither of the AGN candidates are located within the primary $b \leq 100 \text{ kpc}$ sample.

The DEEP2 survey utilizes an apparent magnitude cut

of $B < 24.1$, which at our median redshift corresponds to $M_B - 5\log(h) = -19.6$, ignoring k -corrections (we account for these on a per-galaxy basis below). At the extreme low and high redshift ends of the sample, the limiting absolute magnitude changes by approximately ± 1 . For consistency with low redshift studies we have used $M_B^* = -19.8 + 5\log(h) \approx -20.5$, so the magnitude limit (at $z=0.87$) corresponds to roughly $\sim 0.8L^*$ on this scale. Several galaxies are slightly fainter than this on account of their lower redshift, but the bulk of our sample consists of galaxies with $L \sim 1 - 3L^*$.

3. RESULTS

3.1. Searching QSO Spectra

After the raw frames were processed using MASE, the resulting ten spectra were inspected visually for Mg II absorption doublets at redshifts corresponding to the galaxies associated with each line of sight. Where a doublet was detected, W_r was measured directly from the spectral pixels. Where no doublet was detected, a Gaussian absorption profile was fitted to the data at the redshift of the associated galaxy to estimate a 3σ upper limit. A total of 5 doublets were detected at a z coincident with a DEEP galaxy; for 2 sightlines a pair of galaxies were identified near the absorber's redshift, for a total of 7 associated DEEP galaxies. Five Mg II doublets were detected within the DEEP redshift range but with no corresponding DEEP galaxy, and six additional Mg II systems were found outside of the DEEP2 range. All Mg II detections within the DEEP2 redshift window are listed in Table 2. DEEP objects with no corresponding Mg II detections are listed along with upper limits on their Mg II equivalent width in Table 3.

3.2. Measuring SFR

Since many previous papers have examined the connection between Mg II absorption, galactic winds, and star formation rate (SFR), we measure the SFR of galaxies in our sample. Although the preferred indicator of star formation rate (SFR) is the H α line, this wavelength is redshifted out of all DEEP spectra in our sample. We therefore measure SFR using the emission line luminosities correlations empirically derived in Moustakas et al. (2006), which give SFR as a function of B -band luminosity and either O II or H β line luminosity. We preferentially use H β where available, since it is a more reliable tracer less subject to dust attenuation.

The DEEP spectra are not flux-calibrated so line luminosities cannot be calculated in the normal fashion. We therefore tested two separate methods for determining the SFR from DEEP spectra, and compared for consistency. The first method utilizes an archival flux calibration of the DEIMOS spectrograph, as documented in Lemaux et al. (2009) and on the DEIMOS website⁶. This method has the advantage of producing direct O II line fluxes and luminosities, but, lacking spectrophotometric standard observations, it is not a true flux calibration and is subject to time-dependent variation in weather and instrument conditions. We use this as our primary SFR measure throughout the paper.

The second method, described in Zhu et al. (2009), combines un-fluxed spectra with calibrated photometry

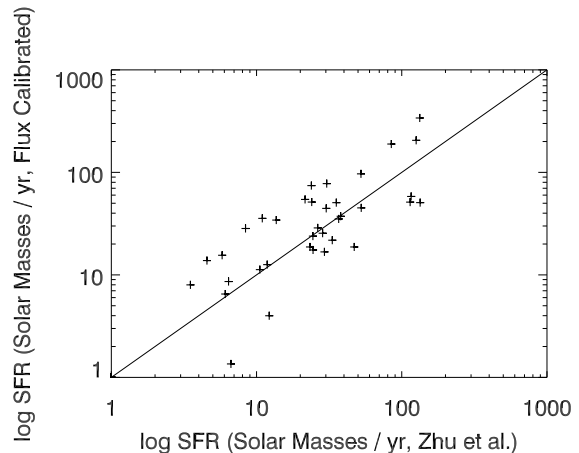


FIG. 4.— Comparison of measurements of the star formation rate using two different methods described in the text.

to bootstrap an estimate of the O II line luminosity. First we measure the equivalent width of the line using an estimated average continuum. We then use *kcorrect*⁷ to reconstruct a galactic SED using the DEEP2 broadband photometry. We take the reconstructed model continuum value at the line, and multiply it by the equivalent width in order to recover the line flux. This flux is then used to calculate the line luminosity and thus SFR. In cases where no emission is detected at the line location, we set the SFR to zero after inspecting the line to ensure it is continuum, since the SFR correlations do not handle nondetections well and produce unreasonably large upper limits.

Figure 4 shows results from both procedures. In general the two methods agree fairly well, having random scatter of $\sim 0.3 - 0.5$ dex but no systematic offsets. Our SFR values ranged between $0.5 \leq \log(\text{SFR} [\text{M}_\odot \text{yr}^{-1}]) \leq 2.0$. AGN are automatically assigned 0 SFR since emission from the AGN renders emission line SFR diagnostics inapplicable. Rest-frame M_B values are also calculated using *kcorrect*; the SFR values and absolute magnitudes are listed in Tables 2 through 5.

3.3. Notes on Individual Systems

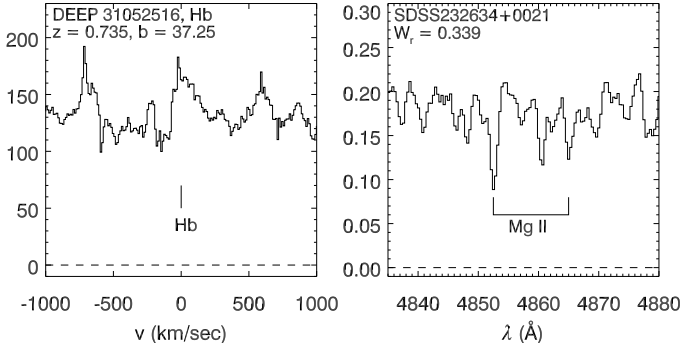
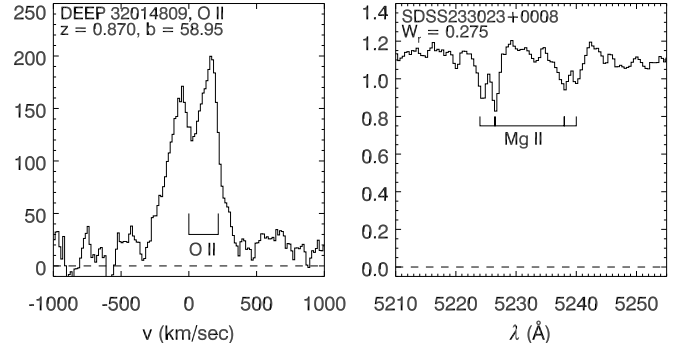
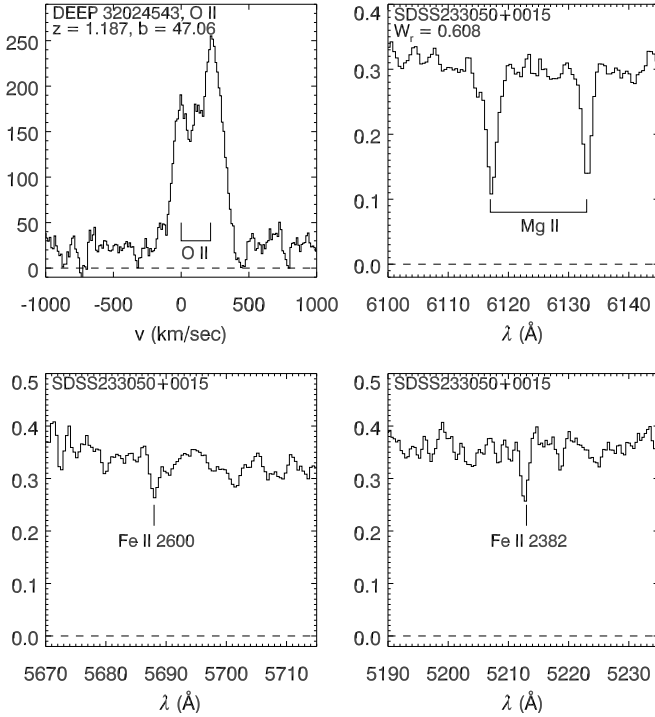
Here we describe properties of the seven sample galaxies hosting Mg II absorption, indicated in Figures 5 through 9. For comparison purposes, we also include plots of the six lowest- b galaxies that had no corresponding Mg II detections in Figure 10. Full spectra of these galaxies are presented in Figure 11 (detections) and Figure 12 (non-detections). All detections have $W_r \leq 0.8 \text{ \AA}$, and all non-detections have 3σ upper limits of $W_{lim} \sim 0.3 \text{ \AA}$. The measured properties of each positively identified galaxy-absorber pair are reported in Table 2. Plots of galaxy spectra are shown in the galaxy's rest frame.

3.3.1. SDSS232634+0021, DEEP 31052516

$z_{gal} = 0.7346$, $b = 37.25 \text{ kpc}$, $W_r = 0.339 \text{ \AA} \pm 0.067$, $\Delta v = -266 \text{ km/s}$ This galaxy's redshift is low enough that the H β line is accessible; however, there is no detected emission at the appropriate wavelength. Rather, we see strong Ca H+K absorption and a 4000

⁶ <http://www.ucolick.org/~ripisc/results.html>

⁷ v.4.2, Blanton & Roweis (2007)

FIG. 5.— Detail of the $z = 0.735$ galaxy-absorber pair.FIG. 7.— Detail of the $z = 0.870$ galaxy absorber pair.FIG. 6.— Detail of the $z = 1.187$ galaxy-absorber pair.

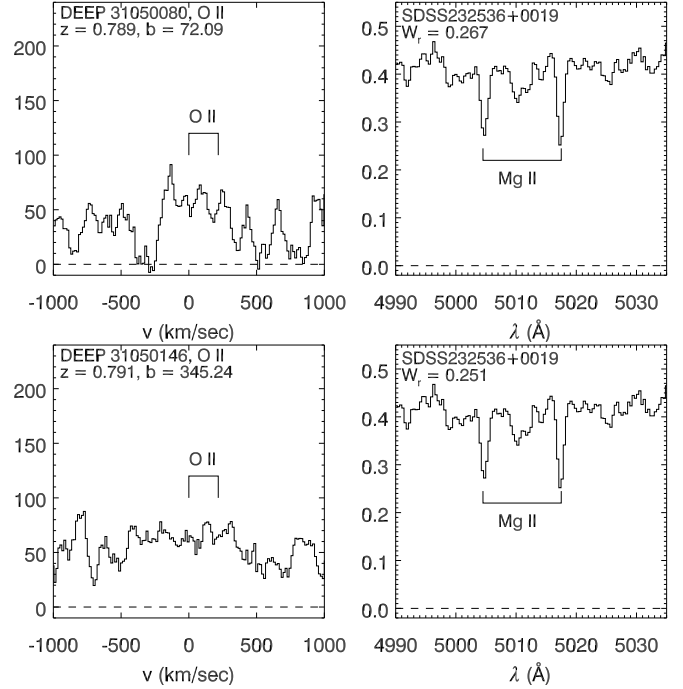
\AA break. This galaxy shows little to no signs of star formation, but with a rest-frame M_B of -21.21, it represents the brightest galaxy in the detected sample; this combined with its spectral features classify it as a luminous red galaxy (LRG). However, despite its low impact parameter (the lowest in the sample) and high intrinsic brightness, its absorption feature is weak.

3.3.2. SDSS233050+0015, DEEP 32024543

$z_{gal} = 1.1875$, $b = 47.06$ kpc, $W_r = 0.608 \text{ \AA} \pm 0.048$, $\Delta v = -95$ km/s DEEP 32024543 displays a strong O II peak, indicative of strong star formation. Its corresponding Mg II absorption feature is strong and narrow, and two additional Fe II lines are visible. The Fe II 2600 line has $W_r = 192 \pm 52$ m \AA , while the 2382 line has $W_r = 129 \pm 46$ m \AA .

3.3.3. SDSS233023+0008, DEEP 32014809

$z_{gal} = 0.8702$, $b = 58.95$ kpc, $W_r = 0.275 \text{ \AA} \pm 0.030$, $\Delta v = 420$ km/s DEEP 32014809's Mg II ab-

FIG. 8.— Detail of the $z = 0.790$ galaxy absorber pair.

sorption line displays an interesting velocity structure, showing not one but two distinct doublets at a corresponding dispersion velocity of ~ 50 km/s, indicating interceptions by two separate clouds of Mg II moving with individual velocities. The galaxy itself displays a strong O II peak indicative of strong star formation.

3.3.4. SDSS232536+0019, DEEP 31050080, 31050146

$z_{gal} = 0.7894/0.7912$, $b = 72.09/345.24$ kpc, $W_r = 0.263 \text{ \AA} \pm 0.040$, $\Delta v = 387/-151$ km/s These two galaxies have very similar redshifts and both exhibit spectral features typical of early-type galaxies, lacking emission at the wavelength of the O II doublet and displaying strong 4000 \AA breaks; these objects may be members of a galaxy group. Although one of these galaxies is at a much lower impact parameter than the other, the galaxies visually bracket the QSO on the sky and the Mg II absorption line is located at a redshift between the two. The absorbing gas may therefore be associated with the group rather than either galaxy specifically. This absorption line also displays an odd asymmetry in

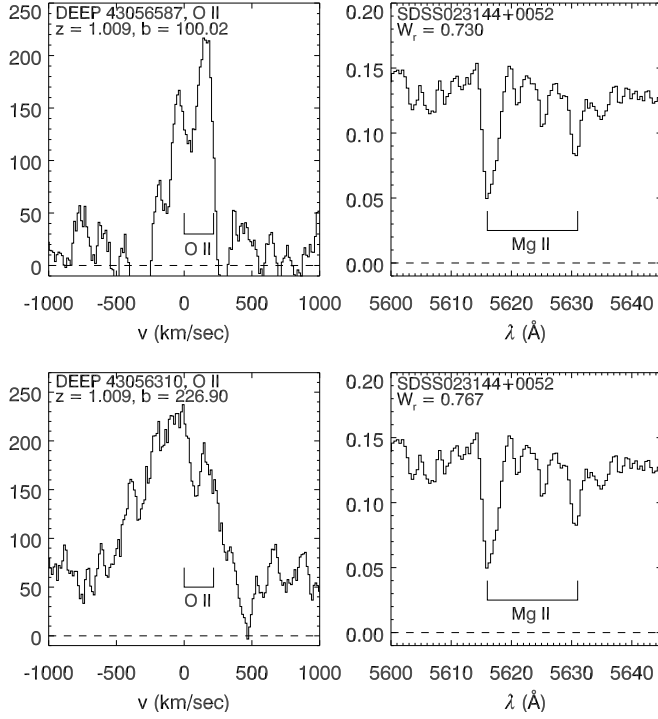


FIG. 9.— Detail of the $z = 1.009$ galaxy absorber pair.

the doublet structure, with the normal ratio of Mg II line depths reversed. This is not an artifact of stacking a bad frame during the reduction process, as the same asymmetry appears in each individual exposure. We examined alternative identifications for this system besides Mg II while enforcing that $0 < z_{abs} < z_{QSO}$, which constrains the rest wavelength to be $2266 < \lambda_{rest} < 5000$ Å ($z_{QSO} = 1.21$). Besides Mg II, the strongest typical QSO absorption lines in this range are from Fe II, which is ruled out based on the non-detection of other multiplet transitions, and Ca II, which is likewise ruled out as a doublet (and would be accompanied by strong DLA-like absorption, which is absent here). Given the exact match in wavelength separation between the components, we suspect the reversed doublet ratio to be the result of contamination by a lower redshift interloper blending with the 2803 Å line.

3.3.5. SDSS023144+0052, DEEP 43056587, 43056310

$z_{gal} = 1.0086/1.0091$, $b = 100.02/226.90$ kpc, $W_r = 0.759$ Å ± 0.067 , $\Delta v = 11/164$ km/s Although only a single strong Mg II absorption doublet is seen in the QSO spectrum, two DEEP galaxies are located at the corresponding redshift. DEEP 43056587 shows a strong O II peak, while DEEP 43056310 displays a broadened O II doublet, but no other characteristic AGN emission lines (e.g. of Ne).

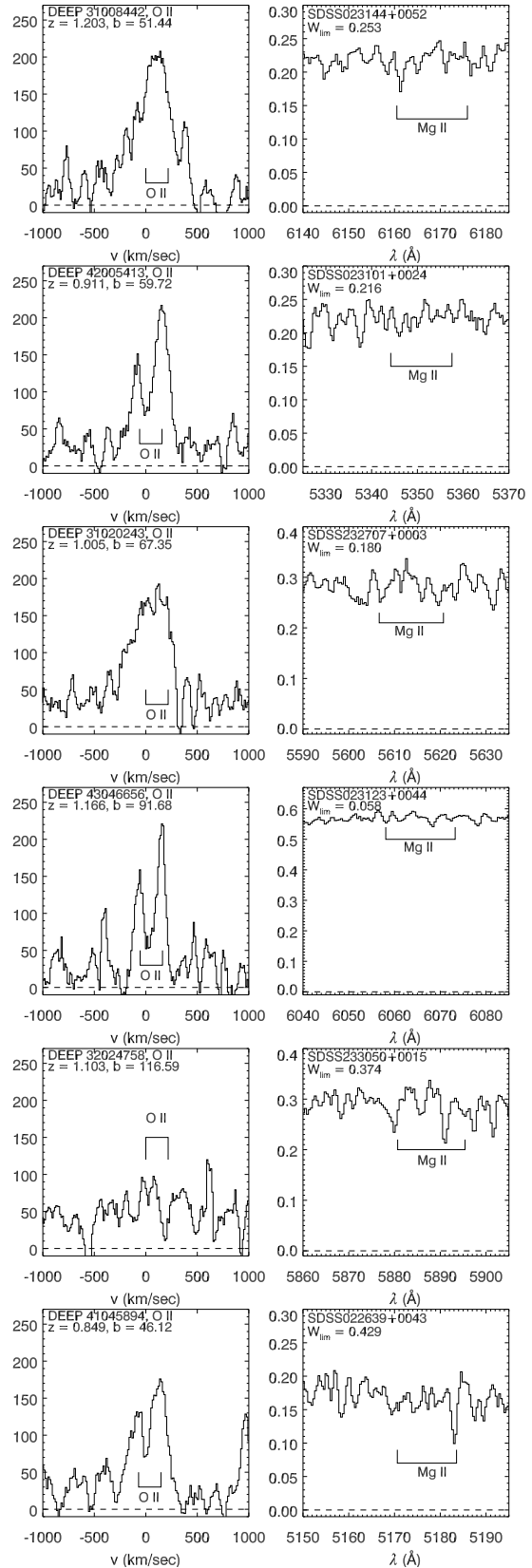


FIG. 10.— Montage of six DEEP2 galaxies with $b \lesssim 100$ kpc, but no detected Mg II. In each case, the left panel shows the [O II] emission line (or $H\beta$ for low redshift), while the right panel displays the Mg II region and associated 3σ upper limit on W_r .

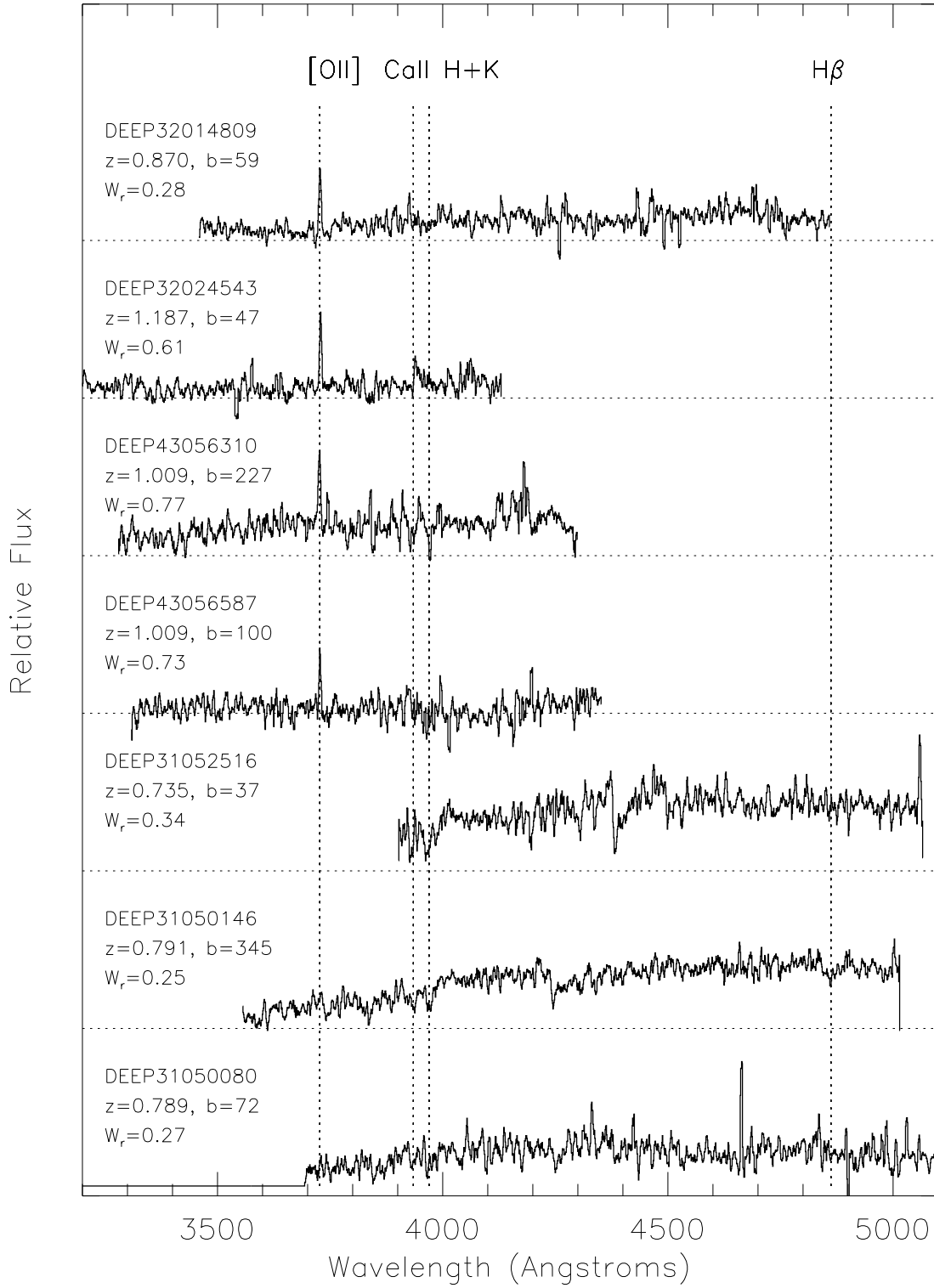


FIG. 11.— DEEP/DEIMOS archival spectra of galaxies associated with Mg II absorption seen in background QSOs. The bottom three galaxies display little evidence of star formation, while the bottom four show moderate activity.

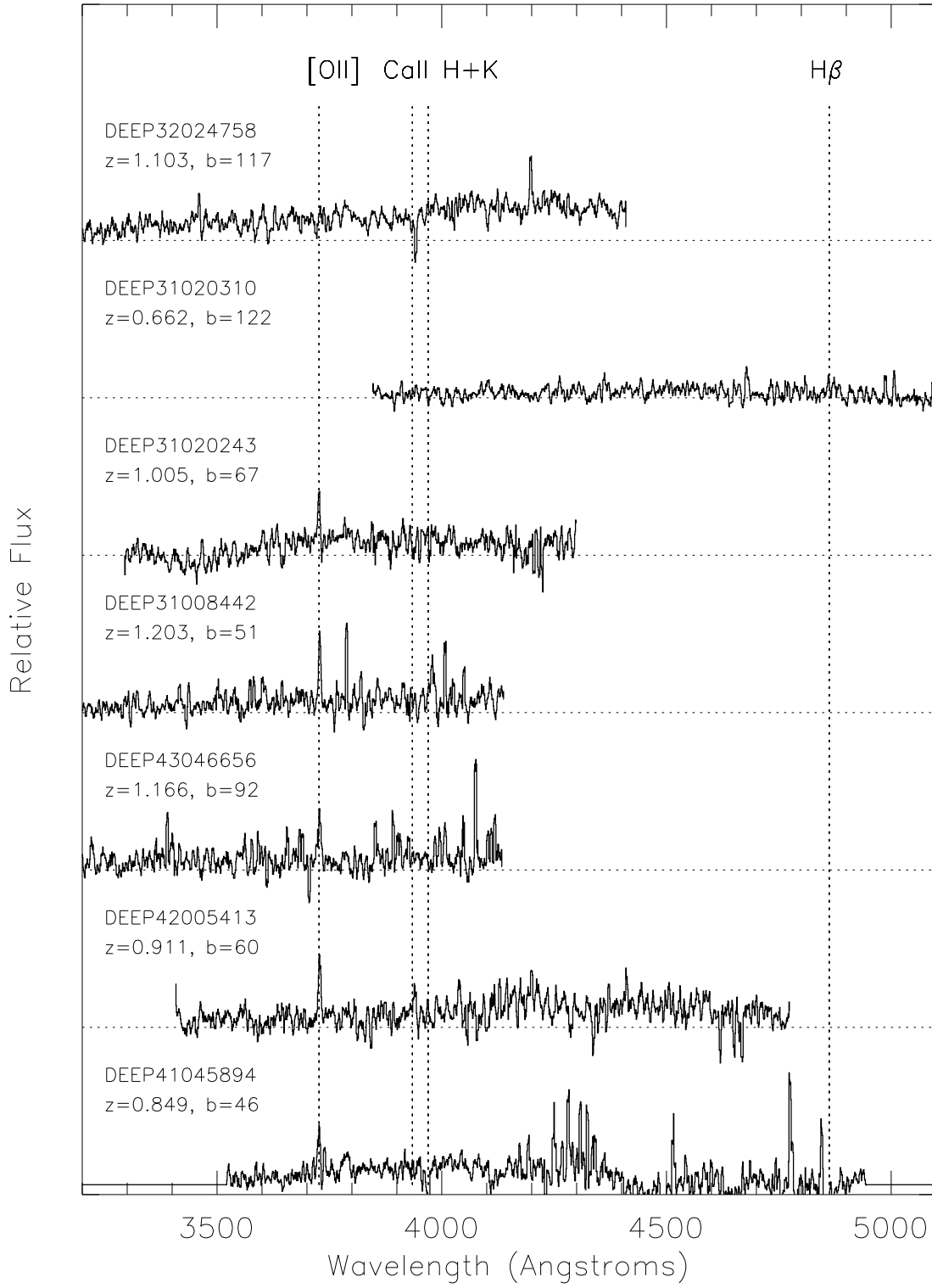


FIG. 12.— DEEP spectra of seven galaxies for which no Mg II was detected in absorption. They are chosen to have the smallest b of the non-absorbing systems, with five of seven at $b < 100$ kpc.

3.4. Trends in Mg II Absorption

3.4.1. Impact Parameter

In Figure 13, we plot the Mg II equivalent widths of our systems against their respective galaxy/QSO impact parameter. The bulk of Mg II detections occur in galaxies with $b \leq 100$ kpc. Beyond this limit, we find no unique galaxy-absorber pairs. In two sightlines we detect absorption at a redshift coincident with a galaxy at large separation; however, in each case there is a second galaxy at $b < 100$ kpc also located at or near the same redshift. Other than this general b limit, no other strong trend emerges.

Simple counting yields a raw covering factor of $\kappa = 50\%$ (5 detections vs. 5 non-detections) at impact parameters $\lesssim 100$ kpc, with $\kappa = 0\%$ at $b > 100$ kpc (discounting the double-galaxy systems). At first glance this matches well with the uncorrected covering fraction of 57% from Chen & Tinker (2008) or 66% from Chen et al. (2010) (Hereafter CT08 and CT10). However, both CT08 and CT10 follow the standard practice (Steidel 1995; Steidel et al. 2002) of renormalizing each pair's impact parameter to account for the fact that larger galaxies should have more extended gas haloes. This is expressed mathematically as an empirical power law scaling between halo radius R_{gas} and galaxy luminosity L_B :

$$R_{gas} = R_{gas}^* \left(\frac{L_B}{L_B^*} \right)^\beta \quad (1)$$

where R_{gas}^* is the fiducial gas radius for an L_B^* galaxy, and β is a constant power law slope; both are determined empirically. Using maximum-likelihood techniques, CT08 estimate $R_{gas}^* = 91 h^{-1}$ kpc, and $\beta = 0.35$ for low z Mg II absorbers. CT08 then consider the covering fraction within R_{gas} rather than raw impact parameter, finding $\kappa = 80 - 86\%$ inside and $\kappa \approx 0$ outside of R_{gas} . The increase in κ from 60% (uncorrected) to 86%

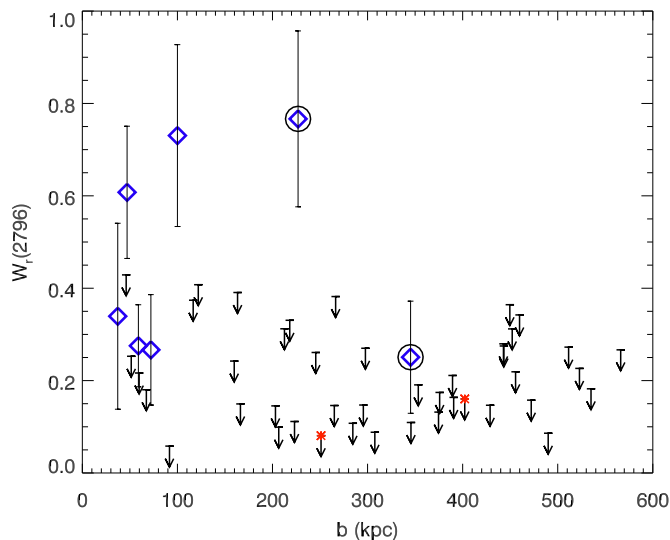


FIG. 13.— Mg II EW vs. impact parameter b . The open diamonds (blue in the color figure) represent detected Mg II absorption. The arrows (black) represent upper limits on possible Mg II absorption. Black circles mark the outer members of galaxy pairs discovered at the absorber redshift. Asterisks (red) mark AGNs. See the electronic edition for a color version of this figure.

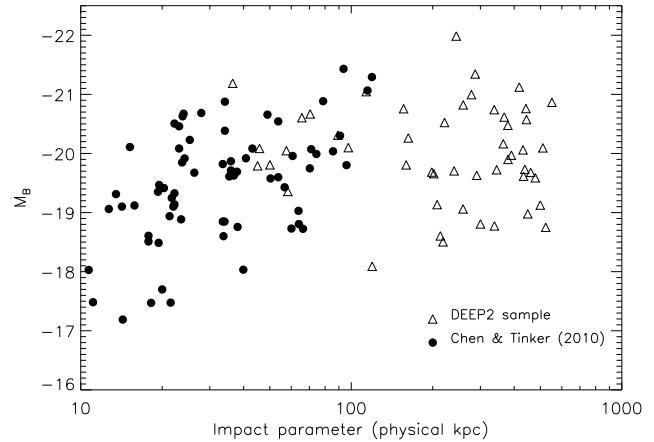


FIG. 14.— Sample comparison between DEEP2 and CT2010, in the impact parameter versus absolute magnitude plane. The CT2010 sample probes further down the luminosity function with particular emphasis on faint systems with $b \leq 20$ kpc that are missed in the high redshift sample.

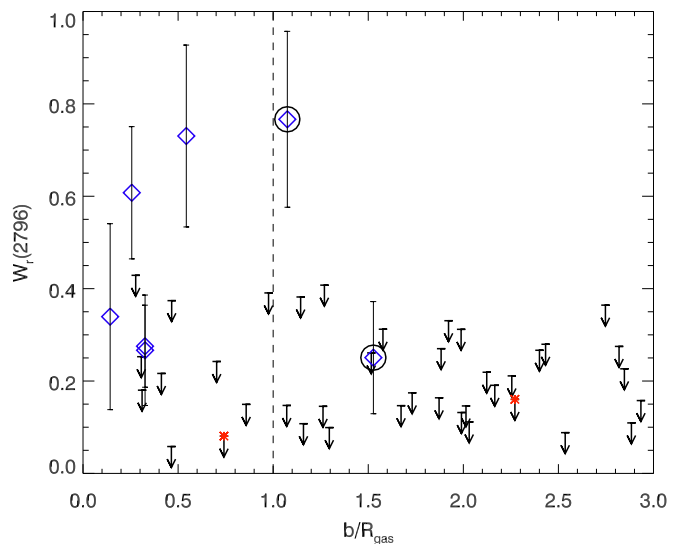


FIG. 15.— Mg II rest equivalent width versus impact parameter in units of R_{gas} , as defined in Equation 1. The horizontal axis has been truncated at 3.0; non-detections in the DEEP sample extend out to $b/R_{gas} = 12$. Diamonds (blue) mark detections, while arrows represent upper limits. Detections with black circles are each co-located in redshift with another sample galaxy having $b/R_{gas} < 1$. Asterisks (red) mark AGN.

(corrected) reflects the fact that many of their Mg II non-detections pair with galaxies of low luminosity. These systems' impact parameters, though less than 100 kpc, still fall outside their (smaller) gas radii.

At DEEP2 redshifts, the situation is reversed because our galaxies are drawn from the brighter end of the luminosity function and therefore reside in larger gas haloes. This is evident from Figure 14, which illustrates the distribution of impact parameter and galaxy luminosity occupied by the low and high redshift samples. As expected, the more nearby surveys are weighted towards low luminosity galaxies at small b .

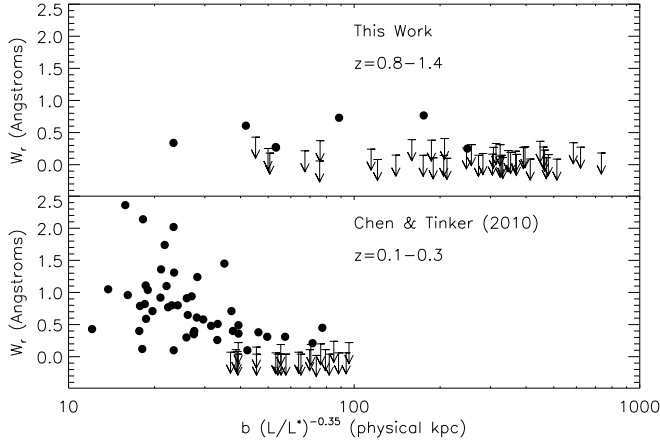


FIG. 16.— Equivalent width versus (luminosity-rescaled) impact parameter for the present sample, compared with that of Chen et al. (2010), illustrating how the high redshift sample skews toward larger impact parameters. Our innermost point has W_r near the low end of CT2010’s envelope, but the samples are otherwise fairly similar. The strongest absorbers in the low redshift sample all arise in systems with rescaled impact parameters smaller than the bulk of the DEEP2 sample. (Note: our point near $b = 50$ kpc represents two detections with similar b and W_r , not separable on the scale of this plot).

In the $z \sim 1$ sample, we find several non-detections located at $b > 100$ kpc (i.e. beyond the approximate gas radius for an L^* galaxy), but which still fall within R_{gas} because the galaxies are bright. This can be seen in Figure 15, where we plot Mg II W_r against impact parameter expressed in dimensionless units of R_{gas} . When evaluating R_{gas} for each system, we correct absolute magnitudes to the rest frame using `kcorrect` and assume $M_B^* = -19.8 + 5 \log(h)$ for consistency with the lower redshift analysis. With this adjustment, the covering fraction at $z = 0.9$ decreases to $\kappa = 38\%$ (5 detections and 8 non-detections within the new R_{gas}).

The lower covering fraction we observe in the high- z sample results at least in part from the fact that these galaxies are located on average at larger impact parameter, where the Mg II W_r and covering factor *should* be lower. Figure 16 illustrates this graphically: the high covering fractions of the CT08 and CT2010 samples are driven by points at rescaled impact parameter < 20 kpc, where the detection probability is essentially unity. Our sample only has one system in this range, and although its W_r is in the bottom 10% of the W_r distribution for $b_{scaled} < 30$ kpc in CT2010, it still represents a positive detection.

The rest of the high redshift sample is at $b(L/L^*)^{-0.35} > 40$ kpc, where the Mg II yield is also low in the low redshift sample. It is clear that the probability of detecting a Mg II absorber varies strongly even inside R_{gas} . This implies that cumulative estimates of κ within a fixed radius depend strongly on the radial selection function of a given sample. Indeed comparisons of κ from one study to another may not be meaningful if not corrected for this effect.

Figure 17 shows the covering fraction for systems grouped into radial bins of 30 kpc. The bin size and shot noise in each bin is large on account of small sample size, particularly at high redshift. But in this view, we

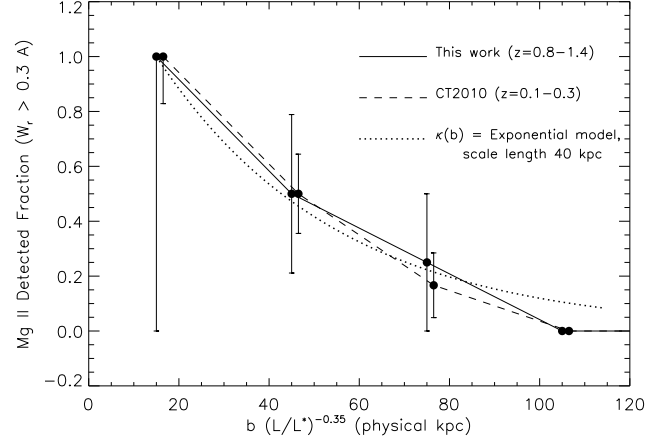


FIG. 17.— Estimates of the differential covering fraction in radial bins, for high and low redshift samples. This quantity expresses the probability of detecting Mg II coincident in redshift with a galaxy as a function of the galaxy-QSO impact parameter. It is a steeply declining function of radius, with a near unity probability at 10-20 kpc dropping to nearly zero at 100 kpc. This figure emphasizes the importance of radial selection functions in calculating meaningful cumulative covering fractions within an arbitrary radius. We find strikingly similar scalings at $z \sim 0.1$ and $z \sim 0.7$, albeit with very large errors at high redshift. Note that in order to avoid double-counting detections associated with pairs of galaxies, we place these detections in the bin corresponding to the b of the closer galaxy.

see that *at fixed galaxy luminosity and impact parameter*, the covering fraction of Mg II absorbers appears to be very similar at $z \sim 0$ and $z \sim 1$, albeit with substantial uncertainties.

The Mg II covering fraction may be expressed very roughly in terms of galaxy impact parameter and luminosity:

$$\kappa(b, L) = \exp \left[\frac{-b(L/L^*)^{-0.35} - 15}{40} \right] \quad (2)$$

This relation is completely empirical, and is not a detailed fit (given the large uncertainties due to sample size). However it does provide some basis for assessing the likelihood that a random galaxy near a QSO sightline will produce Mg II absorption. It also allows for a comparison of samples drawn with different selection functions in luminosity and impact parameter.

3.4.2. Trends with Star Formation Rate

Figure 18 shows a plot of Mg II equivalent width against star formation rate as determined by the methods discussed in section 3.2. Galaxies with impact parameters $b > 200$ kpc are not included for clarity. Although our two strongest absorbers are associated with star forming systems ($30\text{--}100 M_\odot/\text{year}$), there are several other galaxies in the sample with similar SFR but no detected Mg II halo absorption. The systems in our sample lacking emission lines (shown at zero SFR) do harbor comparatively weak Mg II absorbers. In general, any trends in this space are too weak to be revealed by our small sample size.

It may be that passive galaxies are under-represented in the DEEP2 parent sample—especially at high redshift—owing to the photometric preselection and relative redshift success rates. However, as noted by

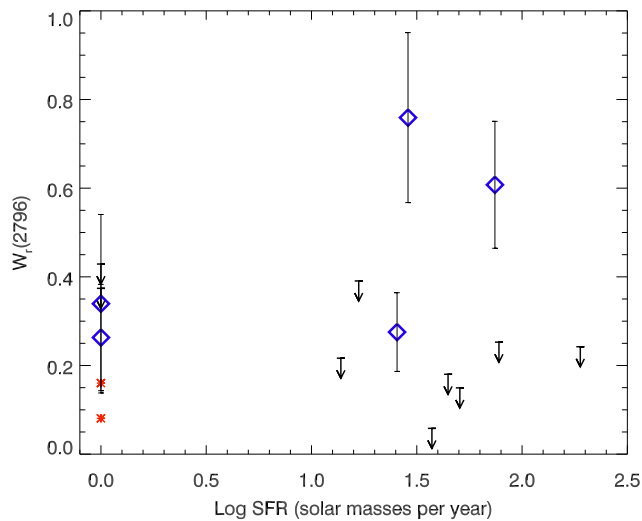


FIG. 18.— Mg II EW vs. $\log(\text{SFR})$. The open diamonds (blue in the color figure) represent detected Mg II absorption. The arrows (black) represent upper limits for Mg II non-detections. Asterisks (red) mark AGN candidates. Only galaxies with impact parameter $b < 100$ kpc are shown. See the electronic edition for a color version of this figure.

Yan et al. (2009), there are substantial populations of the so-called K+A galaxies in $z \sim 1$ samples, indeed we see several such post-starburst systems in the DEEP archive, many with non-negligible O II emission. None are present in our modest Mg II sample, but these galaxies may be a very interesting sample to compare with lower redshifts where they are relatively more rare.

3.5. Trends with Galaxy Type

Within our small sample, we do not detect evidence that Mg II absorption is more commonly associated with either young star forming galaxies or late type stellar populations.

Three of the galaxies with Mg II halo absorption (DEEP31050080, 31052516, and 31050146) display 4000 Å breaks and little to no O II or H β emission (Figure 11). The four remaining galaxies range from moderate to strong star formers, based in part on their O II line emission and weak 4000Å breaks. Two pairs of these galaxies are likely grouped together based on redshift and spatial distribution: the early types 31050080 and 31050146; and the emission line galaxies 43056587 and 43056310. The spectra of seven galaxies with $b \lesssim 100$ kpc but no Mg II detection are shown in Figure 12. These 7 galaxies also cover a range of spectral types: five display O II emission; DEEP 31020310 is low-redshift and does not cover O II, but does show moderate H β and O III; and DEEP 32024758 shows a 4000 Å break.

While we stress that our galaxy sample is unbiased *with respect to DEEP2*, it is important to consider the effects of any bias inherent in the parent sample. DEEP’s photometric pre-selection and apparent magnitude limit, coupled with its improved redshift success rate for emission line galaxies, tends to select star forming systems, particularly at the high redshift end of the sample (Gerke et al. 2007b).

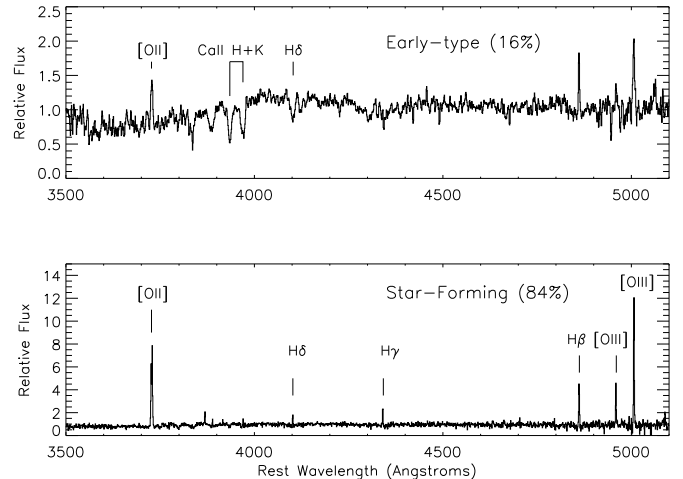


FIG. 19.— Stacked spectra of DEEP2 galaxies classified as Early-type (top) and star-forming (bottom).

To compare the general DEEP2 sample with our Mg II host sample, and also with the general galaxy population, we drew 1000 spectra from the DEEP archive to examine the relative frequency of early- versus late-type galaxies. Spectra with redshifts outside our selection range or in the EGS were not examined. We visually classified each spectrum as either “emission-line dominated,” or “Early-type.” The emission systems displayed strong O II, O III, or H β lines but weak or blue continuum, while the continuum systems showed weaker O II but stronger 4000 Å breaks and Ca H+K absorption. Uniform-weighted rest-frame stacks of the two samples are shown in Figure 19. We found that 84% of the DEEP2 galaxies fell in the emission-dominated category, while 16% were continuum dominated.

In the Mg II-hosting subsample of DEEP2, three of the seven systems (42%) are early-type classifications. This is a modest excess, but we are still in the regime of small number statistics. The Poisson probability of detecting three early-type Mg II hosts (when a randomly drawn sample has an expectation value of slightly over one), is 8%. It appears the Mg II hosts do not differ strongly from the general DEEP2 population. While many Mg II are associated with star-forming galaxies, they certainly do not appear to uniquely be so.

It is less straightforward to quantify how the DEEP2 sample may be biased with respect to a volume limited sample of galaxies at $z \sim 1$. Norberg et al. (2002) performed a similar binary classification of local 2dF galaxies into early- and late-types using principal component analysis, finding roughly equal numbers of the two at our $M^* - 5 \log h = -19.8$. Recall that the DEEP limiting magnitude varies between -18.6 and -20.6 across its full redshift interval. Toward the bright end of our absolute magnitude range, the 2dF late-type fraction decreases to $\sim 30\%$, whereas at the faint end it increases to 70%. However one expects the fraction of blue galaxies to increase toward higher z , particularly in the group environment (Butcher & Oemler 1984; Gerke et al. 2007a).

In short, we find that Mg II absorption is not exclusively associated with a particular spectral type in the DEEP2 galaxy sample. Emission line galaxies and early

type objects alike exhibit Mg II absorption in some cases and not in others. A determination of the exact fraction of early-type versus star forming galaxies hosting Mg II requires an in-depth analysis of sample bias inherent to DEEP2’s selection process; this is beyond the scope of this paper but will be an important question to address when larger samples of Mg II -galaxy pairs are available at $z = 1$. It appears that ongoing star formation is not a prerequisite for populating $z \sim 1$ circumgalactic haloes with cool (i.e. 10^4 K), metal enriched gas; this applies at least for the intermediate values of $0.3 < W_r < 1$ Å typical of galaxy-selected Mg II systems (see Section 4.1).

3.6. Absorbers Without Known Galaxies

Five Mg II systems were found in our QSO spectra with redshifts within DEEP’s selection range ($0.7 < z < 1.4$) but no corresponding match in the DEEP galaxy catalog. We were interested to know if every Mg II absorber could be plausibly associated with a luminous galaxy not captured by DEEP2, or whether some could instead trace galaxies of very low L or intergalactic gas. We therefore searched the DEEP photometric catalogue (Coil et al. 2004) for objects that were detected in imaging but not included in the redshift catalogue because of slit collisions or spectroscopic magnitude limits.

First, we applied the same criteria used by the DEEP survey to select galaxies in the $0.7 < z < 1.4$ range: color cuts of $B - R < 2.35(R - I) - 0.25$, $R - I > 1.15$, or $B - R < 0.5$; magnitude cuts of $18.5 \leq m_B \leq 24.1$; a surface brightness cut of $SB = R_{AB} + 2.5 \log_{10}[\pi(3r_g)^2] \leq 26.5$; and a probability of being a galaxy $p_{gal} > 0.2$. We assumed objects that meet these conditions but have no catalog entry were omitted because of slit conflicts.

We eliminated all objects with QSO impact parameter $b \leq 1''$, as these are likely the QSO itself⁸. We then assumed that every remaining candidate was located at the redshift of the absorption doublet and calculated its physical impact parameter. Two such candidates fell within a 150 kpc radius. They are listed in Table 4. Only one of these seems to be a plausible pair at $b < 100$ kpc.

We then removed the apparent magnitude cut to search for candidates that passed the DEEP color cuts but were deemed too faint for followup, and repeated the calculation. The eleven candidates found this way are listed in Table 5.

Of the four QSO fields containing “bare” Mg II detections, two had candidates not observed because of slit-mask incompleteness. All four fields also had at least one candidate which passed color cuts but was too faint for followup. It is therefore possible that every Mg II system seen in our MagE spectra traces an observable galaxy; i.e. that there are no “bare” Mg II systems.

The one possible exception to this statement is the $z = 0.615$ absorber in SDSS2230+0015 which shows a weak Mg II system ($W_r = 0.148$ Å) but no confirmed galaxies. A pair of faint photometric candidate galaxies separated by $3.8''$ is located at an impact parameter of $21''$ from the QSO. If these are positioned at the redshift of the

absorber, they would pass $b = 143$ kpc from the line of sight, with $18.2h^{-1}$ kpc projected separation and have k -corrected absolute magnitudes $M_B = -16.8$ and -17.8 ($L_B = 0.04 - 0.16L^*$). A third galaxy, also at $b = 21''$ but far from the other two, would have $M_B = -16.4$ ($L_B = 0.04L^*$). No additional galaxies with $L_B > 0.1L^*$ were found within 200 kpc. It appears therefore that this absorber lacks either a faint host galaxy at low impact parameter (i.e. fainter than $\sim 0.05L^*$), or a bright galaxy which could potentially harbor Mg II at large radius. If *both* of the angular pair members are confirmed to lie at the absorber redshift it could provide evidence for gravitational interaction as a mechanism for transporting Mg II to large radii, but without spectroscopic redshifts this interpretation remains speculative.

All other fields all have candidates within 100 kpc, and in some cases several candidates. Followup observations would be required to establish the redshifts of these objects and either confirm or rule out their association with the Mg II absorbers.

In principle one can make qualitative statements about the types of galaxies these candidate galaxies might be based upon DEEP2’s three color photometry and knowledge of the absorber redshift. However, since each of our “bare” Mg II systems has multiple photometric candidates for the host, one cannot make strong statements about the relative contributions of early versus late type galaxies to these unidentified systems.

Nevertheless, we did examine the color properties of each candidate by calculating `kcorrect` templates for each system, placed at the redshift of its corresponding “bare” Mg II absorber. Qualitatively, for galaxies near DEEP2’s central redshift, the $(R - I)$ color measures the strength of the 4000 Å break; galaxies with $(R - I) \gtrsim 0.6$ are more likely to have strong breaks and hence be early type systems, while lower values would select later types. The strength of the $(R - I)$ index decreases at the upper end of DEEP’s redshift range as the 4000 Å break moves through the I band filter. We find two systems whose $(R - I)$ colors (and `kcorrect` templates) favor old stellar populations, and six which favor younger populations, not unlike the main sample. If one lines up candidates at their putative redshift (as determined by Mg II) and assumes that candidates map out a similar region of $(R - I)$ color as the deep spectroscopic sample, then certain candidates become more favorable. When this assumption is applied, then two “bare” Mg II systems are more likely to be hosted by late-type galaxies ($z = 0.684$ in SDSS232634, and $z = 1.477$ in SDSS232707), one is more likely an early-type galaxy ($z = 0.952$ in SDSS232707, and two are inconclusive. At the very least the photometric candidates do not appear to map out a different portion of parameter space.

4. DISCUSSION

Within our small sample, the properties of galaxies giving rise to Mg II absorption are heterogeneous. The likelihood of detecting Mg II absorption appears to scale only with distance and luminosity, and not with star formation or stellar population. We do not see strong evidence that W_r increases at low b , although our coverage is poor at $b \lesssim 30$ kpc where this effect is most pronounced at low redshift. After correcting for galaxy luminosity, the scaling of covering fraction with impact parameter

⁸ One such object, 32024971, at $b = 0.365''$, also had redshift and spectral information in the DEEP archive and was confirmed as the QSO SDSS233050+0015

appears to be very similar at $z \sim 1$ and $z \sim 0$.

While our galaxy population is mixed, none produce absorbers stronger than $\sim 0.8 \text{ \AA}$. Even including absorbers not associated with a DEEP galaxy, our strongest detected absorber has a W_r of only 1.0 \AA , while our weakest is $\sim 0.15 \text{ \AA}$. Previous studies that have identified Mg II absorption with star forming galaxies have also generally selected for high-strength Mg II lines; none of our systems would have been included in these samples. For example, Bouché et al. (2007) found evidence of H α emission correlating to Mg II absorption, but limited the sample to absorbers of $W_r > 2 \text{ \AA}$. Ménard et al. (2009), which correlated Mg II absorption with O II luminosity density, used a lower bound on absorber strength of 0.7 \AA . Zibetti et al. (2007) demonstrated a systematic excess in blue luminosity around quasar sightlines with Mg II absorbers, but again used a lower bound on absorber strength of 0.8 \AA .

By contrast, studies dominated by weaker absorbers (i.e. $W_r \leq 1.0 \text{ \AA}$) do not seem to require this connection between Mg II and star formation in all systems (e.g. Chen et al. 2010). Our Mg II sample compares more closely with this latter group, and our findings are similar. These differing results suggest a divide in the nature of high-strength vs. low-strength absorbers. It may be that high-strength absorbers are direct byproducts of star formation while low-strength absorbers are not. Several authors have previously considered the possibility of multiple Mg II populations: Churchill et al. (2000) segregated these populations by their associated high-ionization absorption, while Nestor et al. (2005) showed tentative statistical evidence of a discrepancy in redshift evolution between strong and weak systems.

4.1. A Weak Evolution in Covering Fraction: Interpretations

Samples of strong Mg II absorbers ($W_r > 1 \text{ \AA}$) show some evidence of association with star formation, while lower W_r samples like ours do not show such a strong trend. It may be that the strong absorbers are a direct consequence of outflows during the actual starburst/outflow phase, while weaker absorbers represent the dispersed remnants of this phase as they settle into the galactic halo. The dispersal could also be aided by tidal disruption or dynamical processes during the halo merging process.

In this picture, the weaker absorbers found in galaxy-selected surveys such as the DEEP2 sample, CT08, and CT2010, represent relics from either earlier episodes of star formation, halo assembly, or both processes together. This would explain the existence of these systems around both early type and late-type galaxies. The strong systems found in absorber-selected surveys such as Bouché et al. (2007), Ménard et al. (2009) and Zibetti et al. (2007), on the other hand, would tend to select more active star forming galaxies.

This interpretation would also explain the redshift evolution in classical, purely statistical Mg II absorber surveys (e.g. Nestor et al. 2005), which show a rapid increase in “strong” absorbers toward higher redshift with a gradual *decrease* in $W_r = 0.3 - 1.0 \text{ \AA}$ absorbers over the same interval. Strong absorbers would track the instantaneous star formation rate and would naturally be

more common during periods of intense star formation. The weak absorbers, by contrast, would gradually accumulate in number with time (toward lower redshift), as they track the integrated star formation rate and/or halo mass assembly. This model also explains the order of magnitude prevalence of weak absorbers over strong ones at all redshifts.

The association of the $W_r < 1 \text{ \AA}$ systems with relic halo gas may account for the relatively weak change in covering properties observed between our $z \sim 1$ sample and similarly constructed $z \sim 0.2$ samples. While CT08 treat Mg II absorption as a generic feature of gaseous halo assembly, they also examine the anticorrelation of halo mass and Mg II W_r (Bouché et al. 2006; Gauthier et al. 2009). Models favoring outflow origins of Mg II explain this anticorrelation as a byproduct of lower mass galaxies having higher star formation and outflow rates; CT08 interpret it as a signature of cold mode accretion (Dekel et al. 2009) of halo gas for low mass systems transitioning to hot mode for higher galaxy masses.

Naively, one would expect that at higher redshifts cold mode accretion would be more prevalent and therefore the covering fraction of Mg II would increase, contrary to our findings. A detailed answer to this question is probably not possible without comparison to simulations, which are challenged to resolve cold flows at redshifts one and zero. Recently Faucher-Giguere & Keres (2010) simulated individual galaxies at high resolution to examine the covering fraction of H I at $z = 2 - 4$. Their calculations showed covering of only a few percent for Damped Lyman-alpha column densities. However for the equivalent of Lyman limit systems—which may be a more fair comparison for Mg II absorbers—the covering fractions range from 10-15%. The calculations did not extend to lower redshifts appropriate for our sample, although the trend indicates that the fraction increases from $z = 2$ to $z = 4$.

One would also expect the overall observed Mg II covering fraction to increase if all Mg II systems are related to star formation. This is particularly true of the strong Mg II systems in the picture we have described above. We have not found such evidence, indicating that our selection method may be less disposed to select Mg II arising from starburst outflows, relative to absorption-line selected galaxy samples.

Tinker & Chen (2010) examine the redshift evolution of the covering fraction using halo occupation models coupled to analytic models of cold accretion. They find a strong redshift dependence of $\kappa \propto (1+z)^{2.75}$ for the *total* Mg II covering from haloes of all galaxy masses. The increase in κ with z is much stronger for haloes below $\sim 10^{11.5} M_\odot$, while more massive haloes do not evolve strongly. We are almost certainly sampling the high end of this mass distribution at high redshift, but we do not see a strong rise in Mg II number counts from undetected low mass galaxies (see Section 3.6). However, if followup spectroscopy demonstrates that the Mg II systems without known galaxies are not paired with any of our photometric candidates—especially the brighter ones missed from slit collisions—then any host galaxy would have to have very low L , lending support to this picture.

4.1.1. Photoionization of Mg II Systems

Broadly, both the cold accretion and starburst outflow would predict an increase in Mg II covering at high redshift which we do not observe. One effect which could counteract this tendency, and has not been discussed extensively in the context of evolution, is the extragalactic ionizing background. The intensity of the UV radiation field rises with increasing redshift between $z = 0$ and $z = 1$, and can eliminate Mg II by ionizing it further to Mg III.

For the galaxies in our sample, we calculated the ratio of local to extragalactic ionizing flux at their individual impact parameter, using each galaxy’s measured absolute magnitude and best fit `kcorrect` model spectral template along with a Faucher-Giguère et al. (2009) ionizing background spectrum. In all cases the extragalactic flux (at the Mg II ionization edge) dominates the illuminating radiation field of the galaxy, by factors ranging from 10 to 10,000, with a median ratio of ~ 1000 .

The degree to which this boost in the UV background ionizes away Mg II depends on the density of the systems as well as their hydrogen column density. We ran simple CLOUDY models to examine this effect over a range of number density, and found that for densities $n_H > 0.05 \text{ cm}^{-3}$ the Mg II equivalent width is mostly unchanged; but for lower values ($n_H \sim 0.001 - 0.01$), the difference in background flux between $z \sim 0$ and $z \sim 1$ could reduce W_r by a factor of 2-3.

The effect of the UV background on $N(z)$ for Mg II could be reduced if the absorbers are optically thick in H I, since the Mg II ionization potential is at only 1.1 Ryd and there is some evidence that Mg II absorbers like the ones seen here relate closely to Lyman limit systems or the outskirts of Damped Lyman alpha systems. For typical column densities seen in LLS or DLA absorbers ($N_{\text{HI}} \sim 10^{18} - 10^{20}$) the densities tested above imply an absorber thickness of order only 100 pc to one kpc. These would seem quite small, but are in fact similar in scale to the sizes of Mg II systems inferred from ionization modeling of individual systems (Charlton et al. 2003) and observations of multiply-imaged gravitational lenses intersecting Mg II haloes (Rauch et al. 2002).

In short, changes in the ionization of Mg II could help explain why the covering fraction at $z \sim 1$ is similar to that at $z \sim 0.2$, despite general expectations that it should rise in cold accretion or outflow models. Ionization and/or photoheating may play a larger role at early times resulting in a small net evolution in κ and $N(z)$ for systems with $0.3 < W_r < 1.0 \text{ \AA}$. Surveys for Mg II at $z > 2 - 3$ (past the peak in the UV background) should help to discriminate between the evolutionary effects of the UV background and gas physics.

4.2. Comparison to dN/dz Estimates for Mg II Systems

We briefly consider the weak evolution in Mg II-galaxy properties in the context of traditional, blind Mg II absorption studies. These large surveys repeatedly find that dN/dz for Mg II *increases* with z (Nestor et al. 2005; Prochter et al. 2006; Steidel & Sargent 1992) slightly faster than a population of sources with constant co-moving density. This requires that either the covering fraction κ increase on a per-galaxy basis, or the number of candidate galaxies increase at earlier times.

Nestor et al. (2005) divide their SDSS Mg II sample into bins of W_r and examine each bin’s evolution separately with respect to the non-evolving case. They find that the majority of the SDSS absorber sample is broadly consistent with no-evolution, and that overall evolution is driven primarily by movement at the strong ($W_r > 3.0 \text{ \AA}$) and weak ($W_r < 0.6 \text{ \AA}$) ends of the W_r distribution. At the strong end, which is not represented in our sample, dN/dz increases toward higher redshift much faster than a non-evolving population; this has been discussed here as well as by Nestor and others in connection with star formation and galactic outflows.

At the low W_r end more appropriate for our sample, Nestor et al. find evidence at the 2σ level for a *decline* in dN/dz —by a factor of ~ 2 for $0.3 < W_r < 0.6$ and $z = 0.5$ to $z = 1$. These results have marginal statistical significance, but they do demonstrate that in the range where our survey is sensitive, evolutionary effects are substantially smaller in weak vs. strong populations in both blind absorption and galaxy-selected surveys.

4.3. Very recent work on Mg II at $z \sim 1$

During review of this paper, Lundgren et al. (2011) presented a complementary analysis of strong Mg II absorbers around DEEP2 galaxies as measured directly from SDSS survey quasar spectra. With a limiting equivalent width of $W_r > 0.6 \text{ \AA}$, this survey is somewhat less sensitive to Mg II absorption and focuses primarily on large scale clustering analysis. Their group reports a 50% covering fraction within $60h^{-1} \text{ kpc}$ (one of two possible systems) and lower covering at larger impact parameters. They detect a large galaxy absorber pair in the spectrum of SDSS0228+0027 (DEEP41013534) with impact parameter $42 h^{-1} \text{ kpc}$ not included in our sample because of priors imposed on observations of background QSOs (the background QSO is at $z = 2.4$). This galaxy is a luminous, clearly early-type system. It further underlines that a non-negligible fraction of Mg II absorbers may be associated with galaxies having low instantaneous star formation rates. Interestingly, this system, like the $z = 0.790$ absorber we report in SDSS2325+0019, may reside in a galaxy group.

In a second recent paper, Bordoloi et al. (2011) examined stacked spectra of ~ 100 foreground-background galaxy pairs in the lower half of our redshift range. While not appropriate for covering fraction measurements, this analysis does produce a mean Mg II equivalent width measurement (for the combined 2796 \AA and 2803 \AA components), which traces the combined effects of absorber strength and covering fraction. The stacked spectrum for all “red” galaxies, which are selected to resemble the early-type systems reported here, yields low W_r for all impact parameters probed, a factor of 2-3 \times below our median, while the “blue” population shows very strong absorption that rises steeply with decreasing radius and increasing stellar mass.

The trends in Bordoloi et al.’s blue sample are crudely consistent with our findings and those of Lundgren et al. (2011) as well as Chen et al. (2010). Their declining stacked W_r at high b may be interpreted as a drop in covering fraction toward higher impact parameters, coupled with a somewhat smaller effect from a decreasing average W_r of each absorber. Comparison of our Figures

16 and 17 roughly reproduce the scalings in Bordoloi’s Figure 4.

The apparent weak absorption from “red” galaxies at all impact parameters is less consistent with the aforementioned galaxy-selected samples. The cause of this discrepancy is not immediately clear; a full accounting will require either larger samples of individual early-type galaxy/absorber systems to measure a detailed covering fraction, or else a separate stack of higher-resolution galaxy spectra to test whether this result based on background galaxies, rather than QSOs, continues to hold.

5. CONCLUSIONS

We have presented a new sample of 10 QSO spectra selected randomly for their proximity to DEEP2 survey galaxies to examine the frequency of Mg II absorption in extended gas haloes at $z \sim 1$. These objects, which each have at least one DEEP2 galaxy at $b < 100$ kpc (and many more at larger b), were observed at medium resolution with the MagE spectrograph. The galaxies have $\bar{z} = 0.87$ and were not chosen for any particular intrinsic properties save for those inherent to the DEEP survey selection criteria.

Our findings may be summarized as follows:

1. Mg II is found in the haloes of early-type and late-type galaxies alike at $z \sim 1$. We see no suggestion of a bias toward any particular stellar population or instantaneous star formation rate. Neither of the two possible AGN in the sample exhibits associated Mg II absorption.
2. We find 5 unique galaxy-Mg II pairs, two of which are grouped with a second galaxy at similar redshift. Five galaxies with DEEP2 spectra at $b < 100$ kpc do not have an associated Mg II absorber.
3. We find five additional Mg II systems in our spectra with no associated galaxy in the DEEP2 catalog. However in all but perhaps one case, a plausible candidate was recovered from the DEEP photometric catalog. These candidates have small impact parameters, but were not observed because of slit mask constraints or a narrow miss of the DEEP2 apparent magnitude cutoff.
4. After applying a simple scaling for galaxy luminosity (i.e. accounting for the idea that more luminous galaxies have more extended haloes), the derived dependence of covering fraction with galaxy impact parameter at $z \sim 1$ becomes strikingly similar to what is observed in similar samples at $z \sim 0.2$. This highlights the importance of accounting for radial sampling functions when calculating the covering fraction of Mg II or other ions within a fixed impact parameter.

The Mg II systems in our sample fall between the regime of the “weak” systems with $W_r < 0.3\text{\AA}$ (Churchill et al. 1999), and the “strong” systems with $W_r > 1\text{\AA}$, the latter of which several groups have suggested may trace galactic outflows. We do not see a strong link between star formation and Mg II incidence, but rather find systems around a wide range of spectral

types. If our intermediate-strength Mg II systems relate to outflows, they may be relic metal-rich material accumulated by either past star formation episodes or dynamical processes occurring during galaxy assembly.

Both the outflow and cold accretion hypotheses would predict an increase in Mg II covering fraction with redshift, which we do not observe. Halo occupation models predict weak evolution for haloes with mass $M > 10^{12}M_\odot$, representative of our sample. However they also predict a sharp rise in Mg II absorption from low mass haloes at higher z which we do not conclusively see. We speculate that the changing extragalactic UV background may play a role in suppressing Mg II absorption at high z , provided 1.1 Ryd photons can penetrate the structures where the absorption occurs.

Observations of Mg II absorption at $z > 2$ may hold some insights into the relationship between halo assembly, star formation, feedback, and ionization evolution. Beyond this redshift, the ionizing background once again declines, which should favor Mg II in the ionization balance. It remains to be seen how this trades off against the decline in abundances at early times. Moreover it is not clear that galaxy scaling relations for L^* systems derived locally would be well justified at such early times. We are exploring this further using IR observations which will extend Mg II number density surveys to $z > 4$.

Facilities: Magellan:Clay (MagE)

We thank Hsiao-Wen Chen for helpful conversations and sharing her data in electronic form, and for conversations with DEEP2 team members, particularly David Rosario. Thanks to Kathy Cooksey for helpful suggestions on an early draft. We thank the staff of Las Campanas Observatory and the Magellan Telescopes for their assistance obtaining the data used here. We also gratefully acknowledge the support of the Sloan Foundation. RAS gratefully acknowledges generous lumbar support from the Adam J. Burgasser Chair in Astrophysics. This work was partly supported by the NSF under grant AST-0908920.

Funding for the DEEP2 survey has been provided by NSF grants AST95-09298, AST-0071048, AST-0071198, AST-0507428, and AST-0507483 as well as NASA LTSA grant NNG04GC89G.

Some of the data presented herein were obtained at the W. M. Keck Observatory, which is operated as a scientific partnership among the California Institute of Technology, the University of California and the National Aeronautics and Space Administration. The Observatory was made possible by the generous financial support of the W. M. Keck Foundation. The DEEP2 team and Keck Observatory acknowledge the very significant cultural role and reverence that the summit of Mauna Kea has always had within the indigenous Hawaiian community and appreciate the opportunity to conduct observations from this mountain.

Funding for the SDSS and SDSS-II has been provided by the Alfred P. Sloan Foundation, the Participating Institutions, the National Science Foundation, the U.S. Department of Energy, the National Aeronautics and Space Administration, the Japanese Monbuka-

gakusho, the Max Planck Society, and the Higher Education Funding Council for England. The SDSS Web Site is <http://www.sdss.org/>.

The SDSS is managed by the Astrophysical Research Consortium for the Participating Institutions. The Participating Institutions are the American Museum of Natural History, Astrophysical Institute Potsdam, University of Basel, University of Cambridge, Case Western Reserve University, University of Chicago, Drexel University, Fermilab, the Institute for Advanced Study, the Japan Participation Group, Johns Hopkins University, the Joint Institute for Nuclear Astrophysics, the Kavli Institute for Particle Astrophysics and Cosmology, the Korean Scientist Group, the Chinese Academy of Sciences (LAMOST), Los Alamos National Laboratory, the Max-Planck-Institute for Astronomy (MPIA), the Max-Planck-Institute for Astrophysics (MPA), New Mexico State University, Ohio State University, University of Pittsburgh, University of Portsmouth, Princeton University, the United States Naval Observatory, and the University of Washington.

TABLE 2
MG II ABSORPTION LINE SYSTEMS AND MATCHED DEEP2 GALAXIES

Quasar Sightline	z_{QSO}^1	DEEP2 Match ²	$z(\text{MgII})$	b^3	M_B^4	SFR^5	W_r^6	$\sigma(W_r)$	Δv^6
SDSS0231+0052	1.61	...	0.820	0.298	0.053	...
		43056587	1.009	100.02	-20.13	26	0.759	0.064	11
		43056310	1.009	226.90	-20.56	112	0.759	0.064	164
SDSS2325+0019	1.21	31050080	0.790	72.09	-20.70	0	0.263	0.040	-150
		31050146	0.790	345.24	-20.77	0	0.263	0.040	387
SDSS2326+0021	1.25	...	0.684	1.041	0.061	...
		31052516	0.735	37.25	-21.21	0	0.339	0.067	-266
SDSS2327+0003	1.75	...	0.952	0.221	0.037	...
		...	1.477	0.419	0.038	...
SDSS2330+0008	1.00	32014809	0.870	58.95	-20.08	29	0.275	0.030	420
SDSS2330+0015	1.94	...	0.615	0.148	0.026	...
		32024543	1.187	47.06	-20.13	24	0.608	0.048	-95

¹ QSO emission redshift

² DEEP2 redshift catalog number for galaxies coincident with $z(\text{MgII})$. Absorbers with no matched galaxies indicated with an ellipsis.

³ QSO-galaxy impact parameter, in h_{71}^{-1} proper kpc

⁴ Rest-frame B band absolute magnitude

⁵ Logarithmic star formation rate, M_\odot/year .

⁶ Rest-frame Mg II $\lambda 2796$ Å equivalent width in Å.

⁷ Absorber-galaxy velocity offset (km/s)

TABLE 3
DEEP GALAXIES AT $b < 250$ KPC WITH NO ASSOCIATED MG II

Quasar Field	z_{QSO}	DEEP Name	z_{gal}	b	M_B	SFR	W_{lim}
SDSS2330+0008	1.00	32014683	0.8049	206.57	-19.69	22	0.099
SDSS0231+0024	1.05	42005413	0.9108	59.72	-19.39	14	0.216
		42005658	0.8278	159.74	-20.79	189	0.242
		42005668	0.8262	166.29	-20.29	50	0.149
		42005439	0.8371	203.12	-19.72	0	0.145
		31049930	1.1573	251.06	-22.03	0	0.081
SDSS2325+0019	1.21	31049930	1.1573	251.06	-22.03	0	0.081
		43046656	1.1661	91.68	-20.35	37	0.058
SDSS0231+0044	1.26	43046720	0.7475	223.14	-18.53	4	0.111
		31008442	1.2027	51.44	-19.85	78	0.253
SDSS2326-0003	1.27	31008442	1.2027	51.44	-19.85	78	0.253
SDSS0231+0052	1.61	43056496	0.8153	245.49	-19.74	51	0.261
SDSS0226+0043	1.66	41045894	0.8488	46.12	-19.82	0	0.429
		41046028	0.8479	212.58	-19.17	0	0.312
		31020243	1.0047	67.35	-20.64	45	0.180
SDSS2327+0003	1.75	31020310	0.6620	121.97	-18.12	13	0.408
		31020364	0.8115	163.24	-19.84	17	0.391
		31019960	0.7400	218.14	-18.63	0	0.331
		32024758	1.1027	116.59	-21.09	0	0.374
SDSS2330+0015	1.94	32024758	1.1027	116.59	-21.09	0	0.374

TABLE 4
DEEP2 PHOTOMETRIC CANDIDATES IN FIELDS WITH UNMATCHED MG II SYSTEMS

Quasar	DEEP Object ¹	θ^2	m_B^3	$(R - I)$	M_B^4	z_{MgII}	b^5	W_r^6
SDSS2326+0021	31052514	9.7	23.59	0.32	-18.45	0.684	68.901	1041
SDSS2330+0015	32024973	21.1	23.88	0.57	-17.83	0.615	143.509	148

¹ DEEP2 catalog number

² Impact parameter (arcsec)

³ Measured, observed frame apparent B magnitude

⁴ Inferred rest frame, k -corrected absolute B magnitude, expressed as $M_B - 5 \log(h)$, assuming that candidate lies at z_{MgII} .

⁵ Inferred impact parameter in h_{71}^{-1} kpc, assuming that candidate lies at z_{MgII} .

⁶ Rest-frame Mg II $\lambda 2796$ Å equivalent width

TABLE 5
FAINT DEEP2/MG II PHOTOMETRIC CANDIDATES EXCLUDED BY APPARENT MAGNITUDE

Quasar Field	DEEP Object ¹	θ^2	m_B^3	$(R - I)$	Inferred M_B^4	z_{MgII}	b^5	W_r^6
SDSS0231+0052	43056354	4.0	24.67	0.56	-18.23	0.820	30.5	323
	43056414	13.3	24.21	0.00	-17.71	0.820	101.5	298
SDSS2326+0021	31052590	18.2	24.22	0.22	-17.65	0.684	129.7	1041
SDSS2327+0003	31019897	2.5	25.25	0.87	-18.56	0.952	20.2	665
	31020185	9.0	24.53	0.19	-18.38	0.952	71.8	221
	31020316	16.7	24.94	0.05	-17.60	0.952	133.5	221
	31019897	2.5	25.25	0.87	-20.94	1.477	21.7	419
	31020185	9.0	24.53	0.19	-19.80	1.477	77.2	419
	31020316	16.7	24.94	0.05	-18.91	1.477	143.4	419
	32024604	21.0	24.59	0.22	-16.80	0.615	143.1	148
SDSS2330+0015	32024616	20.8	25.23	0.12	-16.41	0.615	141.2	148

¹ DEEP2 catalog number

² Impact parameter (arcsec)

³ Measured, observed frame apparent B magnitude

⁴ Inferred rest frame, k -corrected absolute B magnitude, expressed as $M_B - 5 \log(h)$, assuming that candidate lies at z_{MgII} .

⁵ Inferred impact parameter in h_{71}^{-1} kpc, assuming that candidate lies at z_{MgII} .

⁶ Rest-frame Mg II $\lambda 2796$ Å equivalent width

REFERENCES

- Bergeron, J., & Boissé, P. 1991, *A&A*, 243, 344
- Blanton, M. R., & Roweis, S. 2007, *AJ*, 133, 734
- Bochanski, J. J., et al. 2009, *PASP*, 121, 1409
- Bond, N. A., Churchill, C. W., Charlton, J. C., & Vogt, S. S. 2001, *ApJ*, 562, 641
- Bordoloi, R., et al. 2011, *ArXiv e-prints*
- Bouché, N., Murphy, M. T., Péroux, C., Csabai, I., & Wild, V. 2006, *MNRAS*, 371, 495
- Bouché, N., Murphy, M. T., Péroux, C., Davies, R., Eisenhauer, F., Förster Schreiber, N. M., & Tacconi, L. 2007, *ApJ*, 669, L5
- Butcher, H., & Oemler, Jr., A. 1984, *ApJ*, 285, 426
- Charlton, J. C., Ding, J., Zonak, S. G., Churchill, C. W., Bond, N. A., & Rigby, J. R. 2003, *ApJ*, 589, 111
- Chen, H., Helsby, J. E., Gauthier, J., Shectman, S. A., Thompson, I. B., & Tinker, J. L. 2010, *ArXiv e-prints*
- Chen, H., & Tinker, J. L. 2008, *ApJ*, 687, 745
- Churchill, C. W., Mellon, R. R., Charlton, J. C., Jannuzi, B. T., Kirhakos, S., Steidel, C. C., & Schneider, D. P. 2000, *ApJ*, 543, 577
- Churchill, C. W., Rigby, J. R., Charlton, J. C., & Vogt, S. S. 1999, *ApJS*, 120, 51
- Coil, A. L., Newman, J. A., Kaiser, N., Davis, M., Ma, C., Kocevski, D. D., & Koo, D. C. 2004, *ApJ*, 617, 765
- Davis, M., et al. 2003, in Presented at the Society of Photo-Optical Instrumentation Engineers (SPIE) Conference, Vol. 4834, Society of Photo-Optical Instrumentation Engineers (SPIE) Conference Series, ed. P. Guhathakurta, 161–172
- Davis, M., et al. 2007, *ApJ*, 660, L1
- Dekel, A., et al. 2009, *Nature*, 457, 451
- Faucher-Giguère, C., & Keres, D. 2010, *ArXiv e-prints*
- Faucher-Giguère, C., Lidz, A., Zaldarriaga, M., & Hernquist, L. 2009, *ApJ*, 703, 1416
- Gauthier, J., Chen, H., & Tinker, J. L. 2009, *ApJ*, 702, 50
- Gerke, B. F., et al. 2007a, *MNRAS*, 376, 1425
- . 2007b, *MNRAS*, 376, 1425
- Jakobsson, P., et al. 2004, *A&A*, 427, 785
- Jarosik, N., et al. 2010, *ArXiv e-prints*
- Kacprzak, G. G., Churchill, C. W., Ceverino, D., Steidel, C. C., Klypin, A., & Murphy, M. T. 2010, *ApJ*, 711, 533
- Kereš, D., Katz, N., Weinberg, D. H., & Davé, R. 2005, *MNRAS*, 363, 2
- Lemaux, B. C., et al. 2009, *ApJ*, 700, 20
- Lundgren, B., Wake, D., Padmanabhan, N., Coil, A., & York, D. 2011, *ArXiv e-prints*
- Marshall, J. L., et al. 2008, in Society of Photo-Optical Instrumentation Engineers (SPIE) Conference Series, Vol. 7014, Society of Photo-Optical Instrumentation Engineers (SPIE) Conference Series
- Ménard, B., Wild, V., Nestor, D., Quider, A., & Zibetti, S. 2009, *ArXiv e-prints*
- Moustakas, J., Kennicutt, Jr., R. C., & Tremonti, C. A. 2006, *ApJ*, 642, 775
- Nestor, D. B., Johnson, B. D., Wild, V., Ménard, B., Turnshek, D. A., Rao, S., & Pettini, M. 2010, *ArXiv e-prints*
- Nestor, D. B., Turnshek, D. A., & Rao, S. M. 2005, *ApJ*, 628, 637
- Norberg, P., et al. 2002, *MNRAS*, 332, 827
- Prochter, G. E., Prochaska, J. X., & Burles, S. M. 2006, *The Astrophysical Journal*, 639, 766
- Prochter, G. E., et al. 2006, *ApJ*, 648, L93
- Rauch, M., Sargent, W. L. W., Barlow, T. A., & Simcoe, R. A. 2002, *ApJ*, 576, 45
- Steidel, C. C. 1995, in *QSO Absorption Lines*, ed. G. Meylan, 139–+
- Steidel, C. C., Dickinson, M., & Persson, S. E. 1994, *ApJ*, 437, L75
- Steidel, C. C., Kollmeier, J. A., Shapley, A. E., Churchill, C. W., Dickinson, M., & Pettini, M. 2002, *ApJ*, 570, 526
- Steidel, C. C., & Sargent, W. L. W. 1992, *ApJS*, 80, 1
- Tinker, J. L., & Chen, H. 2010, *ApJ*, 709, 1
- Weiner, B. J., et al. 2009, *ApJ*, 692, 187
- Yan, R., et al. 2009, *MNRAS*, 398, 735
- Zhu, G., Moustakas, J., & Blanton, M. R. 2009, *ApJ*, 701, 86
- Zibetti, S., Ménard, B., Nestor, D. B., Quider, A. M., Rao, S. M., & Turnshek, D. A. 2007, *ApJ*, 658, 161